Indian Journal of Chemistry
Vol. 63, January 2024, pp. 105-111
DOI: 10.56042/ijc.v63i1.7908

Direct growth of hierarchically Ni_3S_2 nanostructures on nickel foam for enhanced hydrogen evolution reaction

Xiaokang Zhong[a#], Mure Ali[b#], Xiuting Wang[c], Wanxin Lu[b], Kangle Yong[d], Delong Feng[d], Yun Zhou[d,e,*] & Jie Xu[d,*]

[a] School of Physical Education, Southwest Medical University, Luzhou 646000, China

[b] School of Clinical Medicine, Southwest Medical University, Luzhou 646000, China

[c] College of Intelligent Manufacturing and Automotive Engineering, Luzhou Vocational and Technical College, Luzhou 646000, China

[d] School of Medical Information and Engineering, Southwest Medical University, Luzhou 646000, China

[e] State Key Laboratory for Mechanical Behavior of Materials, School of Materials Science and Engineering, Xi'an Jiaotong University, Xi'an 710049, China

E-mail: yzhou@swmu.edu.cn, xujie011451@163.com

Received 3 August 2022; Accepted (revised) 18 April 2023

Hydrogen is not only a promising energy, but also widely used in inflammation treatment and sports training. The key to these applications is to obtain pure hydrogen conveniently. Water electrolysis provides a green and sustainable method for hydrogen production, but the urgent problem is to develop low-cost and efficient electrocatalysts. In this work, hierarchically porous Ni_3S_2 nanostructures, which the flocculent two-dimensional Ni_3S_2 is coated on the surface of Ni_3S_2 nanosheets, have been successfully grown on nickel foam through a facile two-step hydrothermal reaction. The hierarchically porous Ni_3S_2 nanostructures has a large specific surface area can expose more active sites and facilitates desorption of bubbles. Moreover, the theoretical calculation has indicated that the dimensional confinement effect of metallic Ni_3S_2 improves the carrier concentration and conductivity. Therefore, the hierarchically porous Ni_3S_2 nanostructures on nickel foam have exhibited enhanced hydrogen evolution reaction and good catalytic stability. This work sheds some light on improving the catalytic performance of metallic compounds.

Keywords: Metallic compounds, Hierarchically, Dimensional confinement, Hydrogen evolution reaction

Hydrogen is not only a promising solution for energy, but is also expected to be actively applied to sports training. Some researches indicate that drinking hydrogen water has a certain protective effect on exercise-induced oxidative stress injury, reduce serum malondialdehyde and increase exercise endurance[1-5]. The key to these application scenarios is to obtain pure hydrogen conveniently. Hydrogen production from electrolytic water will be a good choice, but its commercial application is facing the great challenge of lack of low-cost and efficient electrocatalysts[6,7]. In this case, researchers continue to develop alloy or compound electrocatalysts to replace precious metal electrocatalysts. As a kind of promising electrocatalysts for hydrogen evolution reaction (HER), transition metal compounds have attracted extensive research attention in the past few years[8-11]. However, most compounds have poor conductivity, which is not conducive to electrons reaching the surface active sites. On the other hand, poor conductivity will form a Schottky barrier between the interfaces of electrolyte/catalyst or catalyst/support substrate, thus increasing the reaction overpotential[12]. Therefore, some compounds with metallic properties are of particular interest.

Ni_3S_2, a naturally occurring transition metal chalcogenide, acts out intrinsic metallic behaviour due to the continuous Ni-Ni bonds network in the structure[13]. In addition, Ni_3S_2 is also a low cost and easily available compound, which makes it regarded as a potential electrocatalyst for hydrogen evolution reaction[14,15]. Sun *et al.* compared the electrocatalytic hydrogen evolution ability of three nickel sulfur compounds under alkaline conditions, and the results showed that the hydrogen evolution catalytic performance of Ni_3S_2 was better than that of NiS_2 and NiS. They attributed this result to the good conductivity of Ni_3S_2[16]. Since then, various methods have been used to further improve the HER catalytic

# Both the authors contributed equally to the article.

performance of Ni_3S_2, such as element doping, hetero structure construction and so on. But few studies have focused on the design of Ni_3S_2 itself. Considering that the catalytic performance of Ni_3S_2 is sensitive to the morphology, this can be used as a direction of performance optimization[17]. The rational morphology not only expose more active sites of the catalyst, but also facilitate desorption of micro-bubbles from the catalyst surface. Notably, Xu *et al*. found that the density of states of Ni_3N nanosheet at the Fermi level was greater than that of Ni_3N bulk when they were studying the electrochemical water oxidation performance of metallic Ni_3N. It shows that the carrier concentration and conductivity of Ni_3N can be further improved by applying dimensional confinement, thus enhanced the catalytic reaction[12]. It is conceivable that a similar phenomenon can occur when applying dimensional confinement to metallic Ni_3S_2. In other words, reasonable morphology construction has a great impact on the catalytic performance of Ni_3S_2.

Herein, hierarchically porous Ni_3S_2 nanosheets were directly grown on nickel foam (denoted as Ni_3S_2(0.1)/NF) by a simple two-step hydrothemal method. These Ni_3S_2 nanostructures could not only expose more active sites, but also exhibited enhanced carrier concentration and conductivity. As a result of optimization of morphology and electrical characteristics, Ni_3S_2(0.1)/NF displayed improved catalytic performance for hydrogen evolution reaction in alkaline solution. This work sheds some light on the development of metallic compound as low-cost, efficient electrocatalysts for hydrogen evolution reaction.

Experimental Details

The chemical reagents, nickel(II) nitrate hexahydrate ($Ni(NO_3)_2{\cdot}6H_2O$, AR), ammonium fluoride (NH_4F, AR), urea ($CO(NH_2)_2$, AR), sodium sulfide nonahydrate ($Na_2S{\cdot}9H_2O$, AR), hydrochloric acid (HCl, AR), ethanol (CH_3CH_2OH, AR), potassium hydroxide (KOH, EL), commercial Pt/C (20 wt%), distilled water, were used directly without any other treatment in this work. The thickness and bulk density of nickel foam (NF) used in this work were 1.0 mm and 0.45 g/cm^3, respectively.

Synthesis of catalysts

The NF was cleaned successively by ultrasonic with 3.0 M HCl solution, distilled water and ethanol for 10 min before used. Then, a facile two-step hydrothermal method was used to prepare self-standing catalytic electrodes. In the first step, 0.837 g $Ni(NO_3)_2{\cdot}6H_2O$, 0.074 g NH_4F, 0.360 g urea and 70 mL distilled water were prepared into a homogeneous solution, which was then transferred to 100 mL Teflon-lined stainless steel autoclave. A piece of cleaned NF was immersed into the solution and sealed in the autoclave. Placed the autoclave in an electric furnace and heated it to 120 °C for 6 h. After natural cooling to RT, the precursor grown on NF was obtained. In the second step, the as-prepared precursor electrodes were hydrothermally sulfurized at 160°C for 6 h with Na_2S aqueous solution. Finally, the catalytic electrodes were washed with distilled water and ethanol for several times and then dried in vacuum.

Catalysts characterization

XRD patterns were conducted on PANAlytical X'Pert'S-MPD with Cu-Kα radiation (λ=0.154056 nm). SEM and TEM images were obtained from Merlin Compact field emission scanning electron microscopy and JEM-F200 transmission electron microscopy, respectively.

Electrochemical measurements

The electrochemical measurements were carried out using a CorrTest CS350 electrochemical workstation with a standard three-electrode system in 1.0 M KOH solution. The as-prepared catalytic electrodes, Hg/HgO reference electrode and graphite rod were used as the working, reference and counter electrodes, respectively. Before initiation of the tests, electrolyte was saturated by high purity nitrogen for more than 30 min. The polarization curves were recorded by linear sweep voltammetry (LSV) at a scan rate of 5 mV/s. The electrochemical impedance spectroscopy (EIS) was performed at −0.2 V (*vs*. RHE) over the frequencies range from 100 kHz to 1 Hz with an amplitude of 10 mV. The double-layer capacitance (C_{dl}) of catalytic electrodes were measured by cyclic voltammetry at the scan rates of 12, 16, 20, 40, 60, 80 and 100 mV/s in a non-Faradaic region. The catalytic durability of the electrode was studied using a chronopotentiometric method. All the potentials presented were referenced to the reversible hydrogen electrode by adding (0.098 + 0.059 × *p*H) V. iR drop compensation was manually performed for all polarization curves.

Theoretical calculations

The electrical properties variation within the dimensional confinement of Ni_3S_2 was performed

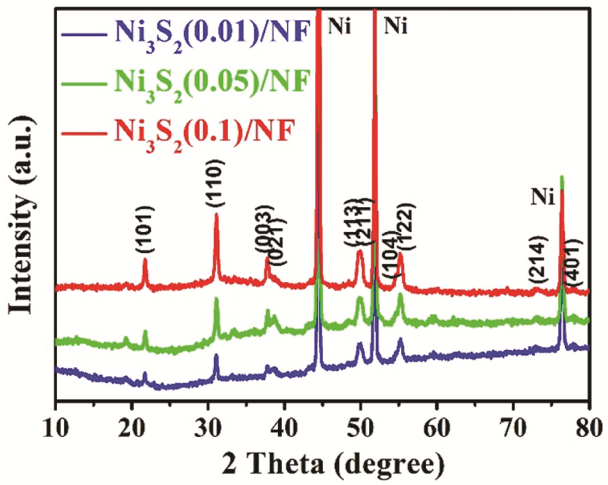

Fig. 1 — The XRD patterns of the as-prepared catalytic electrodes

using density functional theory (DFT) based on the VASP software package. The electron exchange-correlation potential was employed to describe the generalized gradient approximation (GGA) which was developed by Perdew, Burke and Ernzerhof (PBE)[18]. The brillouin zones were sampled by the Monkhorst-Pack scheme with a 2×2×1 k points grid, which had the convergence tolerance of energy of 10^{-5} Ha (1 Ha = 27.2114 eV), maximum force of 0.002 Ha/Å and maximum displacement of 0.005 Å. The vdW interaction was introduced to treat the interaction between the CO molecules and the substrate, and it was described by a semiempirical correction by the Grimme method[19].

Results and Discussion

As mentioned previously, the catalytic electrodes were obtained by a facile two-step hydrothermal method. In detail, the precursor electrodes obtained in the first step were hydrothermally sulfurized with 0.01 M, 0.05 M and 0.1 M Na_2S solution, respectively. The XRD patterns are shown in Fig. 1. It can be seen all the patterns are mainly composed of two phases. Except for three sharp diffraction peaks from NF, the other peaks located at 2θ=21.76°, 31.10°, 37.77°, 38.21°, 49.72°, 50.08°, 54.63°, 55.16°, 73.05° and 77.91° are basically in agreement with (101), (110), (003), (021), (113), (211), (104), (122), (214) and (401) planes of Ni_3S_2 (JCPDS #44-1418), respectively. This result indicates that the surface of catalytic electrodes contains only Ni_3S_2 phase after hydrothermal sulfurization in different concentrations of Na_2S solution. For ease of presentation, the electrodes obtained by hydrothermal sulfurization in 0.01 M, 0.05 M and 0.1M Na_2S solution are named as Ni_3S_2(0.01)/NF, Ni_3S_2(0.05)/NF and Ni_3S_2(0.1)/NF, respectively.

The morphology and microstructure of the as-prepared precursor and catalytic electrodes were observed by SEM and TEM. As shown in Fig. 2a, the precursor with nanosheets was uniformly grown on the surface of NF through the first hydrothermal step. However, the morphology of the precursor electrodes is not alike after hydrothermal sulfurization by different concentrations of Na_2S solution. In the concentration of 0.01 M, the morphology is still nanosheets but slightly curled, as shown in Fig. 2b. When the concentration increased to 0.05 M, the nanosheets are further curled and their surface seems to become rough (Fig. 2c). Interestingly, hierarchically nanosheets were formed in the concentration of 0.1 M. It can be seen some fine flocculent structure covers the surface of the nanosheets (Fig. 2d). More details can be presented by TEM image, which shows the larger nanosheet are coated with two-dimensional thin sheets (Fig. 3a). The high-resolution TEM (HRTEM) in Fig. 3b displays the lattice fringes with interplanar spacings of 0.286 nm, 0.185 nm and 0.235 nm, 0.205 nm corresponding to the (110), (113) and (0210, (202) planes of Ni_3S_2, respectively. This result proves that the hierarchically nanosheets are only composed of Ni_3S_2 phase, which is consistent with the result of XRD. It can be inferred that the formation of hierarchically Ni_3S_2 nanosheets is as follows: In the second step of hydrothermal sulfurization, the anions of the precursors would be replaced by the active sulfur anions (S^{2-}) (Ref. 20) released from Na_2S to form Ni_3S_2. The replacement reaction will not destroy the nanosheet morphology of the precursors. With the increase of the concentration of Na_2S solution, a redox reaction between S^{2-} and NF would also occur. Therefore, flocculent two-dimensional Ni_3S_2 structure is formed on the surface of Ni_3S_2 nanosheets *via* diffusion growth process. Finally, the hierarchically porous Ni_3S_2 nanostructures were obtained. It's remarkable that if the concentration of Na_2S solution is too high, the NF substrate would be oversulfized and broken. From another point of view, it is confirmed that the excess S^{2-} will fully react with NF.

The electrical properties of Ni_3S_2 bulk and Ni_3S_2 sheet were compared by theoretical calculation. Fig. 4a and b is the schematic diagram of the Ni_3S_2 bulk and sheet, respectively. The calculated density of

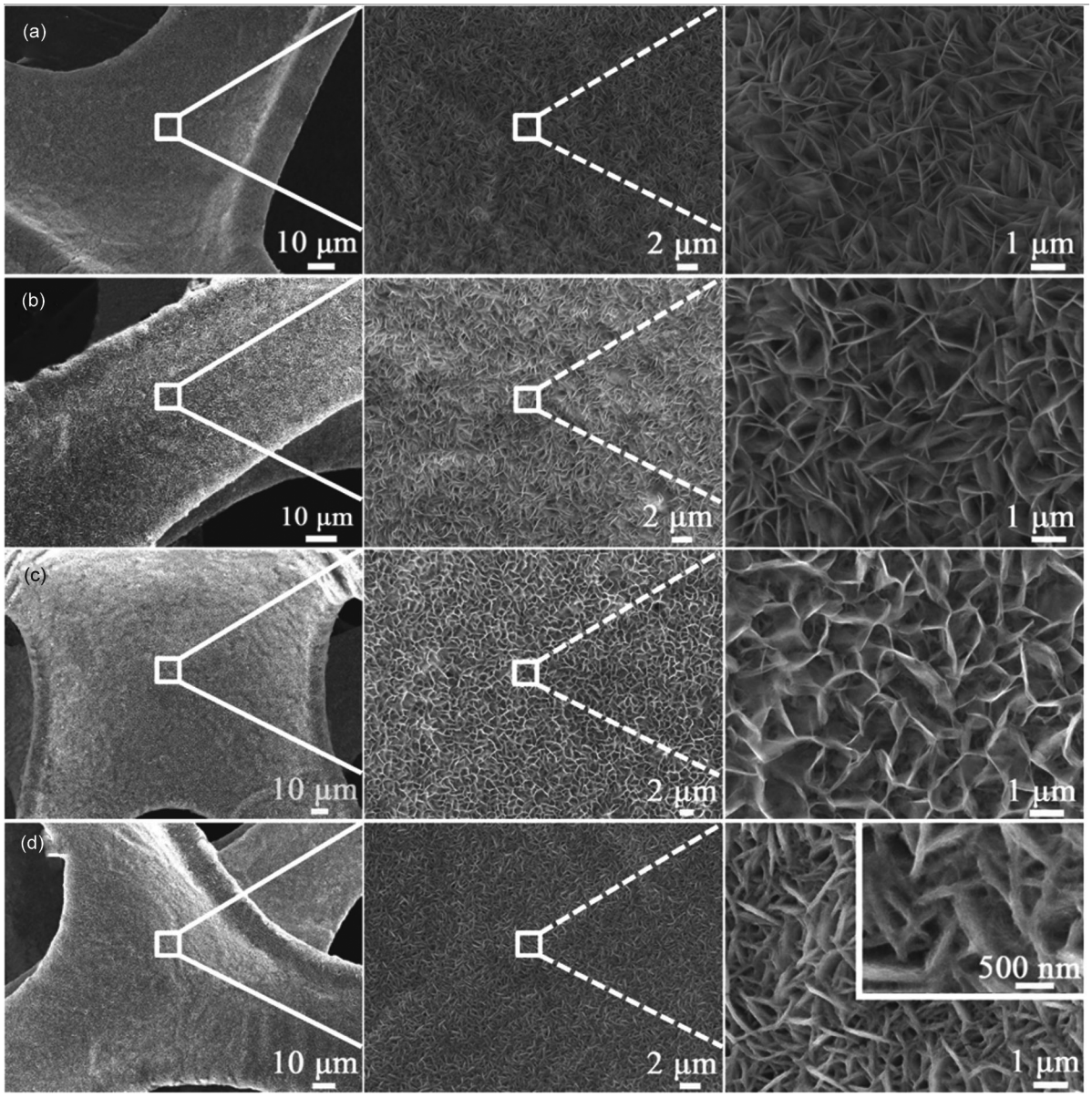

Fig. 2 — SEM images of (a) as-prepared on nickel foam, (b) Ni_3S_2(0.01)/NF, (c) Ni_3S_2(0.05)/NF (c) and (d) Ni_3S_2(0.1)/NF

states (DOS) is shown in Fig. 4c. It can be found that the DOS of both Ni_3S_2 bulk and sheet is continuous at Fermi level, indicating the metallic properties of Ni_3S_2. In addition, the DOS of Ni_3S_2 sheet is larger than that of Ni_3S_2 bulk at the Fermi level, suggesting the dimensional confinement can improve the carrier concentration and conductivity of Ni_3S_2. Therefore, it can be predicted that the two-dimensional Ni_3S_2 on the surface of hierarchically structure possess good electrical properties, which may have a positive impact on the electrocatlysis.

The as-obtained catalytic electrodes can be directly used as binder-free self-supported electrodes for hydrogen evolution reaction. The bare NF and Pt/C-NF were tested as comparison electrodes. As shown in Fig. 5a, there is no doubt that Pt/C-NF exhibits the best performance but bare NF is the worst. It can be seen that Ni_3S_2(0.1)/NF shows enhanced hydrogen evolution reaction performance. It needs overpotentials of 194 mV and 291 mV to drive current densities of 10 mA/cm^2 and 100 mA/cm^2, respectively. However, Ni_3S_2(0.01)/NF and Ni_3S_2(0.05)/NF need much higher overpotentials to reach the same current densities, which are 256 mV, 387 mV and 231 mV, 344 mV, respectively. These results indicate that the hierarchically Ni_3S_2

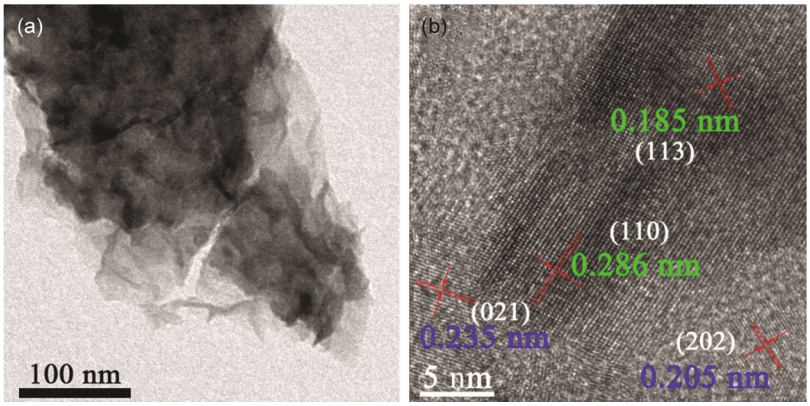

Fig. 3 — (a) TEM and (b) high-resolution images of the hierarchically porous Ni_3S_2 nanostructure

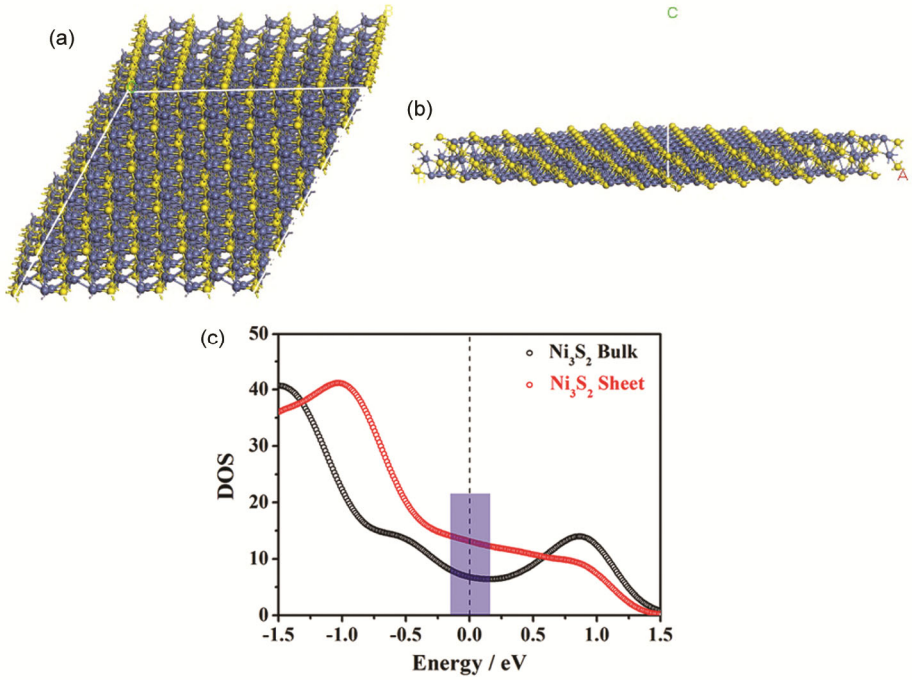

Fig. 4 — Frame diagram of (a) bulk and (b) sheet Ni_3S_2, (c) electronic density of states (DOS) calculated for bulk and sheet Ni_3S_2

nanosheets have obvious superiority in hydrogen evolution reaction.

The Tafel slopes and electrochemical impedance spectroscopy (EIS) were performed to analysis the electrode kinetic. As shown in Fig. 5b, the Tafel slope of Pt/C-NF is 56 mV/dec which agrees with the previously researches. The Ni_3S_2(0.1)/NF possess Tafel slope of 104.1 mV/dec which is much smaller than those of Ni_3S_2(0.05)/NF (120.2 mV/dec), Ni_3S_2(0.01)/NF (141.4 mV/dec) and bare NF (178.1 mV/dec). The smaller Tafel slope value indicates that the catalytic electrode is provided with favorable kinetics of hydrogen evolution reaction[21-23]. Fig. 5c exhibits the Nyquist plots of Ni_3S_2(0.1)/NF, Ni_3S_2(0.05)/NF and Ni_3S_2(0.01)/NF. Both of the plots can be analyzed by an equivalent circuit consisting a series resistance (R_s), a charge transfer resistance (R_{ct}) and a constant phase element (CPE)[20]. The results reveal that the R_s of Ni_3S_2(0.1)/NF, Ni_3S_2(0.05)/NF and Ni_3S_2(0.01)/NF are about 1.0 Ω, which can be attributed to the *in situ* growth on NF. However, the R_{ct} of Ni_3S_2(0.1)/NF (10.6 Ω) is obviously lower than those of Ni_3S_2(0.05)/NF (17.9 Ω) and Ni_3S_2(0.01)/NF (38.5 Ω), suggesting the fastest kinetics of hydrogen evolution reaction between the interface of Ni_3S_2(0.1)/NF and KOH solution [24-26]. It can be

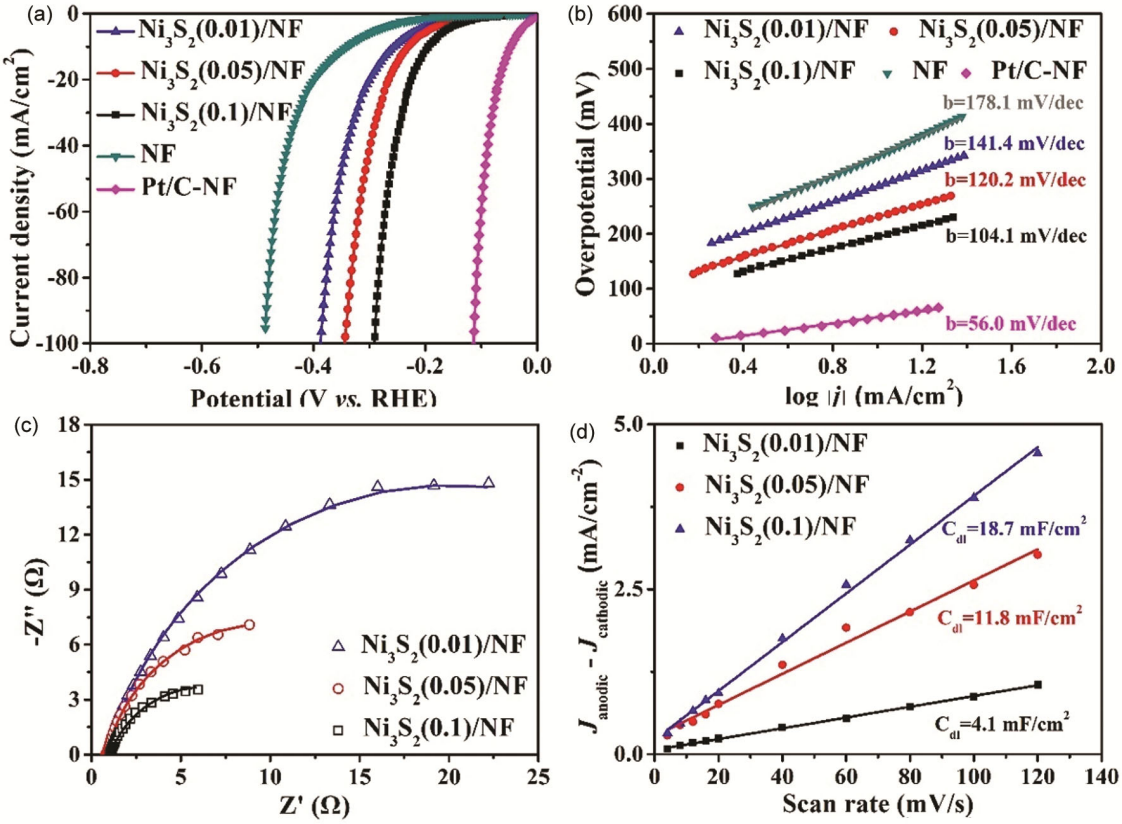

Fig. 5 — (a) LSV curves, (b) corresponding Tafel plots, (c) Nyquist plots and (d) charging current-density difference plotted against scan rate to yield double-layer capacitance (C_{dl}). All of the experiments were carried out in 1.0 M KOH solution

ascribed to the morphological advantage of hierarchically Ni_3S_2 nanosheets, which could not only expose more active sites but also possess good electrical property.

To estimate the electrochemically active surface areas (ECSA) of Ni_3S_2(0.1)/NF, Ni_3S_2(0.05)/NF and Ni_3S_2(0.01)/NF, the electrochemical double layer capacitances (C_{dl}) are investigated, as shown in Fig. 5d. Correspondingly with respect to the order of catalytic activity, Ni_3S_2(0.1)/NF has a C_{dl} (18.7 mF/cm^2) 1.6 and 4.6 times higher than those of Ni_3S_2(0.05)/NF and Ni_3S_2(0.01)/NF, respectively. These results further demonstrate hierarchically Ni_3S_2 nanosheets could provide more active sites for hydrogen evolution reaction.

The stability is an important parameter to reflect the catalytic activity which is explored on a continuous electrolysis using chronoamperometry. Ni_3S_2(0.1)/NF operates for 15 h at a given overpotential that drive an initial current density of 20 mA/cm^2 in 1.0 M KOH solution. As shown in Fig. 6, the result shows that the j-t curve is almost horizontal,

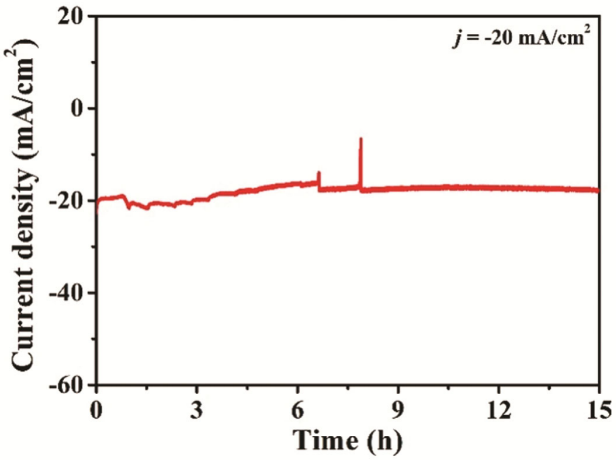

Fig. 6 — Current density *vs.* time (*j*-t) curve of Ni_3S_2(0.1)/NF

just a slight drop takes place. It indicates that Ni_3S_2(0.1)/NF has excellent long-term hydrogen evolution reaction catalytic durability in alkaline medium. The structure of hierarchically porous Ni_3S_2 nanosheets on NF is favourable for the release of gathering bubbles.

Conclusion

In conclusion, hierarchically porous Ni_3S_2 nanosheets were directly grown on nickel foam *via* a simple two-step hydrothermal reaction. During the second step of hydrothermal surfurization, the active S^{2-} release from Na_2S would replace the anions of precursors to form Ni_3S_2, which is a process without destroying the morphology of precursors thus obtaining Ni_3S_2 nanosheets. When increasing the concentration of Na_2S solution (reach to 0.1M), there is not only a replacement reaction, but also a redox reaction between S^{2-} and NF. Then, the flocculent two-dimensional Ni_3S_2 structure is formed on the surface of Ni_3S_2 nanosheets to obtain hierarchically porous Ni_3S_2 nanostructures. The hierarchically porous Ni_3S_2 nanostructures has a large specific surface area can expose more active sites and facilitates desorption of bubbles. Moreover, the dimensional confinement effect of metallic Ni_3S_2 improves the carrier concentration and conductivity, which is favourable to electrocatalysis. Therefore, Ni_3S_2(0.1)/NF exhibits enhanced hydrogen evolution reaction. This work sheds some light on improving the catalytic performance of metallic compounds.

Acknowledgement

This work was supported by the Science and Technology Strategic Cooperation Programs of Luzhou Municipal People's Government and Southwest Medical University (Grant No. 2019LZXNYDJ18).

References

1 Anantharaj S, Noda S, Jothi V R, Yi S C, Driess M & Menezes P W, *Angew Chem Int Edit*, 60 (2021) 18981.
2 Gao Y, Chen Z, Zhao Y, Yu W, Jiang X, He M, Li Z, Ma T, Wu Z & Wang L, *Appl Catal B-Environ*, 303 (2022) 120879.
3 Ostojic S M, *Inter J Sports Med*, 36 (2015) 273.
4 Kawamura T, Higashida K & Muraoka I, *Oxid Med Cell Longevi*, (2020) 2020, (https://doi.org/ 10.1155/2020/ 2328768).
5 Ostojic S M, Vukomanovic B, Calleja-Gonzalez J, *Postgrad Med*, 126 (2014) 188.
6 Du W, Shi Y, Zhou W, Yu Y & Zhang B, *Angew Chem Int Edit*, 60 (2021) 7051.
7 Chen S & Pan Y, *J Phys Chem C*, 125 (2021) 11848.
8 Zhang Y, Hui Z X, Zhou H Y, Zai S F, Wen Z, Li J C & Yang C C, *Chem Eng J*, 429 (2022) 132012.
9 Yin J, Jin J, Zhang H, Lu M, Peng Y, Huang B, Xi P & Yan C H, *Angew Chem*, 131 (2019) 18849.
10 Zhang J, Liu Y, Sun C, Xi P, Peng S, Gao D & Xue D, *ACS Energy Lett*, 3 (2018) 779.
11 Huang C, Yu L, Zhang W, Xiao Q, Zhou J, Zhang Y, An P, Zhang J & Yu Y, *Appl Catal B-Environ*, 276 (2020) 119137.
12 Xu K, Chen P, Li X, Tong Y, Ding H, Wu X, Chu W, Peng Z, Wu C, Xie Y, *J Am Chem Soc*, 137 (2015) 4119.
13 Feng L L, Yu G, Wu Y, Li G D, Li H, Sun Y, Asefa T, Chen W & Zou X, *J Am Chem Soc*, 137 (2015) 14023.
14 Tong X, Li Y, Ruan Q, Pang N, Zhou Y, Wu D, Xiong D, Xu S, Wang L & Chu P K, *Adv Sci*, 9 (2022) 2104774.
15 Zhao Y, You J, Wang L, Bao W & Yao R, *Inter J Hydrogen Energ*, 46 (2021) 39146.
16 Jiang N, Tang Q, Sheng M, You B, Jiang D & Sun Y, *Catal Sci Technol*, 6 (2016) 1077.
17 Ouyang C, Wang X, Wang C, Zhang X, Wu J, Ma Z, Dou S & Wang S, *Electrochim Acta*, 174 (2015) 297.
18 Grimme S, *J Comput Chem*, 27 (2006) 1787.
19 Perdew J P, Burke K & Ernzerhof M, *Phys Rev Lett*, 77 (1996) 3865.
20 Sivanantham A, Ganesan P & Shanmugam S, *Adv Funct Mater*, 26 (2016) 4661.
21 Yang Y, Zhang K, Lin H, Li X, Chan H C, Yang L & Gao Q, *ACS Catal,* 7 (2017) 2357.
22 Wen L, Yu J, Xing C, Liu D, Lyu X, Cai W & Li X, *Nanoscale*, 11 (2019) 4198.
23 Peng S, Li L, Zhang J, Tan T L, Zhang T, Ji D, Han X & Cheng F, *J Mater Chem A*, 5 (2017) 23361.
24 Zhang L, Wang T, Sun L, Sun Y, Hu T, Xu K & Ma F, *J Mater Chem A*, 5 (2017) 19752.
25 Wang K, Zhou C, Xi D, Shi Z, He C, Xia H, Liu G & Qiao G, *Nano Energy*, 18 (2015) 1.
26 Yu J, Li Q, Chen N, Xu C Y, Zhen L, Wu J & Dravid V P, *ACS Appl Mater Inter*, 8 (2016) 27850.